A predictive robust cascade position-torque control strategy for Pneumatic Artificial Muscles

Lotfi Chikh, Philippe Poignet, François Pierrot, Micaël Michelin

A predictive robust cascade position-torque control strategy for Pneumatic Artificial Muscles

Lotfi Chikh †, Philippe Poignet ‡, François Pierrot ‡ and Micaël Michelin †

***Abstract*—A robust cascade strategy is proposed and tested on an electropneumatic testbed for parallel robotic applications. It is applied on Pneumatic Artificial Muscles (PAMs). Nonlinear models are developed and presented. By specifying the pressure average between the two muscles, it is possible to control the torque by controlling the pressure in each muscle. A constrained LMI based $\mathcal{H}_\infty$ controller is synthesized for the pressure inner loop. A computed torque is applied on the torque loop and a Generalized Predictive Controller (GPC) controller is then applied to control position of the muscles. Experimental results show the feasibility of the control strategy and good performances in terms of robustness and dynamic tracking.**

***Index Terms*—GPC, cascade control, pneumatic actuators, modeling, LMI, feedback linearization, robust control, $\mathcal{H}_\infty$, PAMs.**

I. Introduction

The paper is motivated by pick-and-place parallel robotic applications: the study of 1-dof pneumatic actuation system is a preliminary stage which enables us to evaluate performances of Pneumatic Artificial Muscles (PAMs). Parallel robots have a lot of advantages which have made their success. Particularly, they are very fast as the actuators are transferred to the rigid frame reducing considerably the inertia of the moving links and increasing speeds and accelerations of the end effector. For instance, the fastest industrial robot in the world -the Quattro- has a parallel structure and can reach an acceleration of $15g$ [1]. Recently, the Par2 robot which is not industrialized yet has reached $43g$ while keeping a low tracking error [2]. However, a major obstacle for parallel robots expansion is their expensive price due to the cost of the embedded motors which they use. In this context, the inspection of other actuation type such as pneumatic actuators is a matter of fact as they are cheap actuators with low maintenance costs, and good force/weight ratio. As the big obstacle of industrial use of pneumatic actuation in robotics is difficulty in their control, this paper focuses on this particular point.

Numerous techniques have been studied in literature and among them a large part concerns robust control. Robust controllers are necessary to deal with uncertainties and to ensure high precision positioning. They have been applied as a nonlinear feedback using sliding modes by [3] for a planar 2 DOF manipulator. In [4], authors explored adaptive control techniques for parallel robotic applications. One of the problems of nonlinear controllers is difficulty in the synthesis of the control law and the high computational amount. That is why some authors have tested linear robust control techniques such as [5] where PAMs are tested in an antagonist manner. In [5], an $\mathcal{H}_\infty$ controller is synthesized basing on a linear identified nominal system which greatly limits the control performances. This explains why [6] has synthesized an $\mathcal{H}_\infty$ controller after application of feedback linearizing [7] [8] of the nonlinear system. However, only one muscle is controlled and the antagonist case is not studied.

In this paper, a novel robust cascade strategy which combines an outer position predictive controller and an inner torque controller is proposed. The torque controller is based on the $\mathcal{H}_\infty$ pressure control in each muscle after specifying an average pressure into the muscles and a desired torque reference. This desired torque reference is given by the outer position loop. Cascade control has been studied in case of PAMs by [9] and [10]. In this two studies, only simple controllers are applied. In our case, we extend the cascade control concept to robust controllers and predictive ones. The different experimental tests show the advantages of this approach, in terms of good time responses and ability of tracking of extended range references (up to $\pm 25°$). Another motivation of predictive control is that in a precedent study on pneumatic cylinders [11], it was shown that predictive cascade concept can improve robustness performances comparing to state of art control techniques such as sliding modes. The control synthesis is simplified as system is linearized using feedback linearizing techniques [8] [7]. A Generalized predictive controller (GPC) is synthesized for the outer loop and as the system is linear, an explicit solution exists for the predictive optimization problem. The obtained controller is an easy-to-implement one. As far as we know, only two experimental studies of GPC -on pneumatic cylinders and not on PAMs- have been carried out so far [12] [13]. In [12], the model used is a linear one which limits greatly the performances of the controller. In [13], the authors used a model estimation based on neural network theory [13]. No application of GPC basing on an explicit nonlinear model has been found in literature. An intuitive motivation of using predictive theory in pick and place robotic applications is that the trajectories are determined *a priori* and therefore, future trajectory is known. By specifying the pressure average between the two muscles, it is possible to control the torque by controlling pressure in each muscle. A constrained LMI based $\mathcal{H}_\infty$ controller is synthesized for the pressure inner loop. It is based on LMI optimization [14] [15]. In addition to the classical advantages of $\mathcal{H}_\infty$ [16] [17] control in terms of robustness, disturbance rejection, systematic

† Authors are with Fatronik France Tecnalia, Cap Omega Rond-point B. Franklin, 34960 Montpellier Cedex 2, France. lchikh@fatronik.com and mmichelin@fatronik.com

‡ Authors are with the Laboratoire d'Informatique, de Robotique et de Microélectronique de Montpellier (LIRMM). 161 rue Ada, 34392 Montpellier Cedex 5, France. poignet@lirmm.fr and pierrot@lirmm.fr

synthesis of MIMO controllers and powerful combination of both frequency domain synthesis and state space synthesis, the LMI approach enables the addition of constraints in an intuitive manner. Therefore, pole placement constraints have been added to the $\mathcal{H}_\infty$ performances in order to have a better control of the transitory temporal behavior of the pressure controller.

This paper is organized as follows. Section II presents the versatile electropneumatic testbed for robotic applications and its nonlinear modeling. Section III deals with the control of the muscles. After introducing the feedback linearizing equations, both of GPC controller background and LMI based $\mathcal{H}_\infty$ multi-objective approach are introduced. The cascade strategy which combines these two control techniques is then introduced. Finally in section IV, the robust cascade strategy is implemented experimentally and different control tests, including robustness tests, are presented and deeply analyzed.

II. Experimental Pneumatic testbed and nonlinear modeling

The versatile electropneumatic setup is presented in Fig. 1. It includes two 5/3-way proportional valves[1] and three kinds of actuators. The first one is a standard double acting cylinder which is very widespread in industry and one of the cheapest actuators. The second one is the rodless cylinder which has the advantage of being symmetric, that is to say, the maximum force provided in one direction equals the one in the inverse direction. Finally, Pneumatic Artificial Muscles[2] (PAMs) which are deeply studied in this paper.

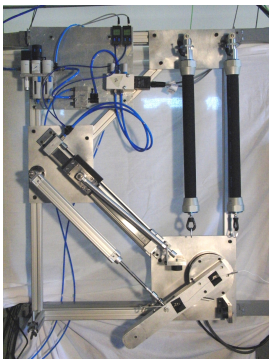

Fig. 1. Versatile electropneumatic setup for robotic application.

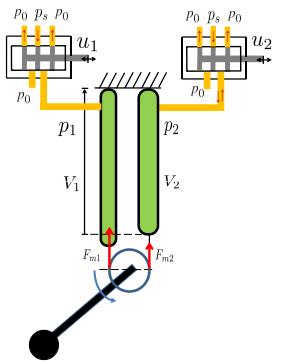

Fig. 2. Schematic representation of the experimental setup.

Both of the two muscles are connected to a moving arm which may represent a robot arm. In the long run, our aim is to design efficient parallel robot which rely on pneumatic actuation with robust control: the moving arm of this test bed is very similar to arms used for various parallel robots such as Delta or Quattro robots. At its extremity, different masses can be attached for robustness tests of the controllers. Three types of sensors are used; a high resolution incremental encoder, two pressure sensors and two force sensors. The real time prototyping environment is xPC Target^{TM} from Mathworks. In the sequel, we present the nonlinear model of the pneumatic muscles. Every electropneumatic positioning device includes an actuation element (the pneumatic cylinder), a command device (the valve), and a mechanical part and position, pressure and/or force sensors. A schematic representation of the electropneumatic system is given in Fig. 2. Supply pressure p_s is supposed to be constant. p_0 denotes the atmospheric pressure. It is supposed that any variation of the muscle's volume or pressure can be described by the polytropic gas law [18]:

$$p_1 V_1^\gamma = p_2 V_2^\gamma \tag{1}$$

Where p_i is the pressure in one of the muscle chamber (indexes 1 and 2 are related to two pressure states) and V_i is the volume in the muscle chamber, γ is the polytropic constant. The ideal gas equation describes the dependency of the gas mass:

$$m = \frac{pV}{rT} \tag{2}$$

where m is the gas mass inside the cylinder chamber or the muscle, T is the air temperature which is considered to be equal to the atmospheric temperature and r is the specific gas constant. Therefore, combining (1) and (2) leads to the pressure dynamic expression:

$$\frac{dp}{dt} = \frac{\gamma}{V(s)}[rTq_m(u,p) - p\frac{dV}{ds}\dot{s}] \tag{3}$$

where u represents the input voltage of the valve, s is the position of the piston in case of the cylinders. $q_m(u,p)$ represents the mass flow rate ($\frac{dm}{dt} = q_m(u,p)$). Dynamic effects of the underlying position controller for the valve-slide stroke are neglected. These hypothesis justify why the mass flow is a function of the input voltage and the pressure in the actuator chamber. The experimental curve representing the volume/stroke dependency is represented on figure 3. According to this characteristic, the volume/stroke model has

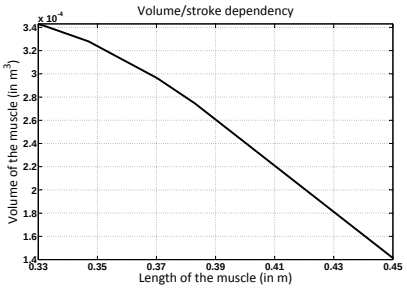

Fig. 3. Volume Stroke dependency

been approximated by a third order polynomial using least squares:

$$V(s) = \sum_{i=0}^{3} b_i s^i \tag{4}$$

The second term of (3) is now completely defined; the first term requires modeling of the valve. The valve model has been

[1]MPYE-5-1/4-010-B from FESTO
[2]PAMs: FESTO MAS - 20-450N-AA-MC-K

approximated -after identification- by the following expression (see [19] for details):

$$q_m(u,p) = \varphi(p) + \psi(p)u \tag{5}$$

φ and ψ defines 5^{th}-order polynomials with respect to p.
For cascade control experiments, it is mandatory to determine the force/pressure dependency. For the muscles, force depends on pressure and also on contraction. The force is maximum when there is no contraction. As the contraction increases the generated force decreases in a non linear way. The experimental measured force characteristic is represented on Fig. 4. It is approximated by the following function:

$$F_m(p,s) = (p - p_0)\sum_{i=0}^{5} c_i s^i \tag{6}$$

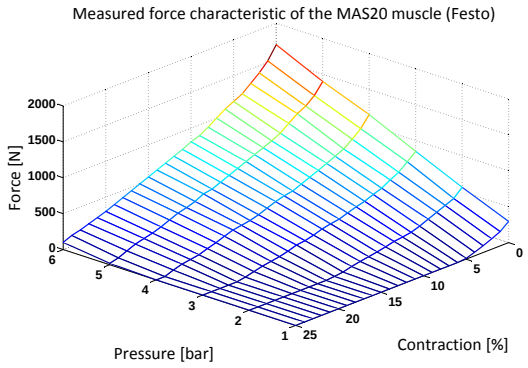

Fig. 4. MAS20 force characteristic

III. Control of the Pneumatic Artificial Muscles

In this section, we first present the feedback linearization equations for the PAMs. The approach handled here can be justified by differential geometry concepts [7] and differential flatness theory [8]. Once the linearized system obtained, two advanced control techniques are presented: GPC and LMI based constrained $\mathcal{H}_\infty$.

A. Feedback linearization equations

It can be easily proved -in case of mass flow rate rate m_g as an input and the pressure difference as an output- that differential flatness criteria is satisfied and that the system is completely linearizable (using differential geometry concepts [7]). The pressure dynamic in each muscle is given by:

$$\frac{dp}{dt} = \frac{\gamma r T}{V(s)}\dot{m}_g - \frac{\gamma}{V(s)}\frac{dV}{ds}\dot{s}p \tag{7}$$

If we take,

$$\dot{m}_g = \frac{V}{\gamma r T}(u_{aux} + \frac{\gamma}{V}\frac{dV}{ds}\dot{s}p) \tag{8}$$

This leads to the following linearized system:

$$\dot{p} = u_{aux} \tag{9}$$

The linearized system is then a first integrator. The pressure controller which is synthesized basing on this first integrator is presented in the next section.

B. Multi-objective output feedback pressure control via LMI optimization

An LMI is any constraint of the form:

$$A(x) = A_0 + x_1 A_1 + \ldots + x_N A_N < 0 \tag{10}$$

where $A_0 \ldots A_N$ are given symmetric matrices and $x^T = (x_1 \ldots x_N)$ is the vector of unknown variables. In (10), the symbol $<$ refers to negative definite [3].
One way of tuning simultaneously the $\mathcal{H}_\infty$ performance and transient behavior is to combine $\mathcal{H}_\infty$ and pole placement objectives using LMI optimization techniques. Poles are clustered in regions which can be expressed in terms of LMIs. The class of LMI region defined below has been introduced for the first time by [15]. It turns out to be suitable for LMI-based synthesis.
Def. LMI Regions. A subset $\mathcal{D}$ of the complex plane is called an LMI region if there exists a symmetric matrix $\alpha = [\alpha_{kl}] \in \mathbf{R}^{m\times m}$ and a matrix $\beta = [\beta_{kl}] \in \mathbf{R}^{m\times m}$ such that:

$$D = \{z \in \mathcal{C} : f_{\mathcal{D}}(z) < 0\} \tag{11}$$

with: $f_{\mathcal{D}}(z) := \alpha + z\beta + \bar{z}\beta_T = [\alpha_{kl} + \beta_{kl} z + \beta_{lk}\bar{z}]_{1\le k,l\le m}$.
For instance, we use a disk LMI region centered at $(-q, 0)$ with radius r. It is defined below [15]:

$$f_{\mathcal{D}}(z) = \begin{bmatrix} -r & q+z \\ q+\bar{z} & -r \end{bmatrix} < 0 \tag{12}$$

The constrained $\mathcal{H}_\infty$ problem under consideration can be stated as follows [15]. Given an LTI plant:

$$\begin{aligned} \dot{x}(t) &= Ax(t) + B_1\omega(t) + B_2 u(t) \\ e(t) &= C_1 x(t) + D_{11}\omega(t) + D_{12}u(t) \\ y(t) &= C_2 x(t) + D_{21}\omega(t) + D_{22}u(t) \end{aligned} \tag{13}$$

an LMI stability region $\mathcal{D}$, and some $\mathcal{H}_\infty$ performance $\gamma > 0$, find an LTI control law $u = K(s)y$ such that: (1) the closed-loop poles lie in $\mathcal{D}$ and (2) $\|T_{we}\|_\infty < \gamma$ where $\|T_{we}(s)\|$ denotes the closed-loop transfer function from ω to e. It is represented on Fig. 5. where the input vector $\omega = \begin{pmatrix} b & v \end{pmatrix}^T$

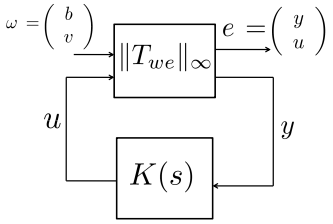

Fig. 5. System representation and notations

can be constituted for instance by a disturbance b and a second input which can be a measure noise v. The output vector $e = \begin{pmatrix} y & u \end{pmatrix}^T$ is composed by the controlled output y and the control signal u. In our case, and as defined latter in (37), y is the pressure difference between the chambers and u is the

[3] the largest eigenvalue is negative

input voltage.
The controller transfer function is denoted $K(s)$ and can be represented in the following state-space form by:

$$\begin{aligned} \dot{x}_K(t) &= A_K x_K(t) + B_K y(t) \\ u(t) &= C_K x_K(t) + D_K y(t) \end{aligned} \tag{14}$$

Then, $T_{wz}(s) = D_{cl} + C_{cl}(sI - A_{cl})^{-1}B_{cl}$ with[4]: $A_{cl} = \begin{pmatrix} A + B_2 D_K C_2 & B_2 C_K \\ B_K C_2 & A_K \end{pmatrix}$, $B_{cl} = \begin{pmatrix} B_1 + B_2 D_K D_{21} \\ B_K D_{21} \end{pmatrix}$, $C_{cl} = (C_1 + D_{12} D_K C_2, D_{12} C_K)$
and $D_{cl} = D_{11} + D_{12} D_K D_{21}$.

We first examine each specification separately. It is shown in [15] that the pole placement constraint is satisfied if and only if there exists $X_{\mathcal{D}} > 0$ such that:

$$[\alpha_{kl} X_{\mathcal{D}} + \beta_{kl} A_{cl} X_{\mathcal{D}} + \beta_{lk} X_{\mathcal{D}} A_{cl}^T]_{1 \le k,l \le m} < 0 \tag{15}$$

Meanwhile, the $\mathcal{H}_\infty$ constraint is expressed in terms of LMIs:

$$\begin{pmatrix} A_{cl} X_\infty + X_\infty A_{cl}^T & B_{cl} & X_\infty C_{cl}^T \\ B_{cl}^T & -\gamma I & D_{cl}^T \\ C_{cl} X_\infty & D_{cl} & -\gamma I \end{pmatrix} < 0 \tag{16}$$

Then the problem formulation of $\mathcal{H}_\infty$ synthesis with pole placement - assuming that the same Lyapunov matrix $X > 0$ is required - is:

$$\begin{aligned} &\text{Find } X > 0 \text{ and a controller } K(s) > 0 \equiv \Omega_K \text{ that satisfy} \\ &(15) \text{ and } (16) \text{ with } X = X_{\mathcal{D}} = X_\infty \end{aligned} \tag{17}$$

The controller matrix is denoted by:

$$\Omega_K = \begin{pmatrix} A_K & B_K \\ C_K & D_K \end{pmatrix} \tag{18}$$

The difficulty in output feedback is that relations (15) and (16) involve nonlinear terms of the form $\mathcal{B}\Omega_K\mathcal{C}X$. This means that problem formulation is not convex and then, can not be handled by LMIs. Chilali and Gahinet [15] solved this problem by taking the following change of variables of the controller:

$$\begin{aligned} \mathcal{B}_K &= NB_K + SB_2 D_K \\ \mathcal{C}_K &= C_K M^T + D_K C_2 R \\ \mathcal{A}_K &= NA_K M^T + NB_K C_2 R + SB2C_K M^T \\ &+ S(A + B_2 D_K C_2) R \end{aligned} \tag{19}$$

where R, S, N and M correspond to the following partition of X and it inverse as

$$\begin{aligned} X = \begin{pmatrix} R & M \\ M^T & U \end{pmatrix}, X^{-1} = \begin{pmatrix} S & N \\ N^T & V \end{pmatrix} \\ R \in \mathbf{R}^{n \times n}, S \in \mathbf{R}^{n \times n} \end{aligned} \tag{20}$$

The proposed procedure is summarized in the following theorem [15]:
Theorem1:
Let $\mathcal{D}$ be an arbitrary LMI region contained in the open left-half plane and let (11) be its characteristic function. Then, the modified problem (17) is solvable if and only if the following system of LMIs is feasible.
Find $R = R^T \in \mathbf{R}^{n \times n}$, $S = S^T \in \mathbf{R}^{n \times n}$, and matrices $\mathcal{A}_K$, $\mathcal{B}_K$,$\mathcal{C}_K$ and D_K such that

$$\begin{pmatrix} R & I \\ I & S \end{pmatrix} > 0 \tag{21}$$

$$\left[\alpha_{kl} \begin{pmatrix} R & I \\ I & S \end{pmatrix} + \beta_{kl} \Phi + \beta_{lk} \phi^T \right]_{k,l} < 0 \tag{22}$$

$$\begin{bmatrix} \Psi_{11} & \Psi_{21}^T \\ \Psi_{21} & \Psi_{22} \end{bmatrix} < 0 \tag{23}$$

with the shorthand notation

$$\Phi := \begin{pmatrix} AR + B_2 C_K & A + B_2 D_K C_2 \\ \mathcal{A}_K & SA + \mathcal{B}_K C_2 \end{pmatrix} \tag{24}$$

Ψ_{11}, Ψ_{12} and Ψ_{22} terms are detailed in [15]. Given any solution to this LMI system:

- Compute via Singular Values Decomposition (SVD) a full-rank factorization $MN^T = I - RS$ of the matrix $I - RS$ (M and N are then square invertible)
- Solve the system of linear equations (19) for B_K, C_K and A_K (in this order).
- Set $K(s) = D_K + C_K(sI - A_K)_{-1}B_K$.

Then $K(s)$ is an *n*th order controller that places the closed-loop poles in $\mathcal{D}$ and such that $\|T_{wz}\|_\infty < \gamma$.

C. GPC outer position Controller

The GPC algorithm is based on a CARIMA model which is given by:

$$A(z^{-1})y(t) = z^{-d}B(z^{-1})u(t-1) + C(z^{-1})e(t) \tag{25}$$

where $u(t)$ and $y(t)$ are respectively the control and output sequences of the plant and e(t) is a zero-mean white noise. A, B and C are polynomials of the backward shift operator z^{-1}. They are given by; $A(z^{-1}) = 1 + a_1 z^{-1} + a_2 z^{-2} + ... + a_{na} z^{-na}$, $B(z^{-1}) = b_0 + b_1 z^{-1} + b_2 z^{-2} + ... + b_{nb} z^{-nb}$ and $C(z^{-1}) = 1 + c_1 z^{-1} + c_2 z^{-2} + ... + c_{nc} z^{-nc}$ and $\triangle = 1 - z^{-1}$. For simplicity, it is admitted that C^{-1} equals 1. It is important to mention that most SISO plants can be described by a CARIMA model after linearization. The GPC algorithm consists in applying a control sequence that minimizes a multistage cost function of the form:

$$\begin{aligned} J(N_1, N_2, N_u) = &\sum_{j=N_1}^{N_2} \delta(j)[\hat{y}(t+j|t) - w(t+j)]^2 \\ &+ \sum_{j=1}^{N_2} \lambda(j)[\triangle u(t+j-1)]^2 \end{aligned} \tag{26}$$

where $\hat{y}(t+j|t)$ is an optimum j step ahead prediction of the system output on data up to time t, N_1 and N_2 are the minimum and maximum costing horizons, N_u is the control horizon, $\delta(j)$ and $\lambda(j)$ are weighting sequences and $w(t+j)$ is the future reference trajectory.
The minimization of cost function leads to a future control sequence $u(t), u(t+1), ...$ where the output $y(t+j)$ is close to $w(t+j)$. Therefore, in order to optimize cost function, the

[4] we assume that the $D_{22} = 0$, this assumption considerably simplifies the formulas. (Note that it is always possible to remove the D_{22} term by a mere change of variables)

best optimal prediction of $y(t+j)$ (for $N_1 \leq j \leq N_2$) has to be determined. This needs the introduction of the following Diophantine equation:

$$1 = A_j(z^{-1})\tilde{A}(z^{-1}) + z^{-j}F_j(z^{-1}) \tag{27}$$

with $\tilde{A} = \triangle A(z^{-1})$ and polynomials E_j and F_j are uniquely defined with degrees $j-1$ and na respectively. $\triangle$ is defined as $\triangle = 1 - z^{-1}$

By multiplying (25) by $\triangle E_j(z^{-1})z^j$ and considering (27), we obtain:

$$\begin{aligned} y(t+j) =& F_j(z^{-1})y(t) + E_j(z^{-1})B(z^{-1})\triangle u(t+j-d-1) \\ &+ E_j(z^{-1})e(t+j) \end{aligned} \tag{28}$$

Since the noise terms in (28) are all in the future (this is because degree of polynomial $E_j(z^{-1}) = j-1$), the best prediction of $y(t+j)$ is:

$$\hat{y}(t+j|t) = G_j(z^{-1})\triangle u(t+j-d-1) + F_j(z^{-1})y(t) \tag{29}$$

where $G_j(z^{-1}) = E_j(z^{-1})B(z^{-1})$

Polynomials E_j and F_j can merely be obtained recursively (demonstration can be found for instance in [20]).

In the future, it will be referred only to $N = N_2 = N_u$ as the prediction horizon. N_1 is chosen equal to 0.

Let's consider the following set of j ahead optimal predictions:

$$\begin{aligned} &\hat{y}(t+d+1|t) = G_{d+1}\triangle u(t) + F_{d+1}y(t) \\ &\vdots \\ &\hat{y}(t+d+N|t) = G_{d+N}\triangle u(t+N-1) + F_{d+N}y(t) \end{aligned} \tag{30}$$

It can be written in the following compact form:

$$\mathbf{y} = \mathbf{G}\ \mathbf{u} + \mathbf{F}(z^{-1})y(t) + \mathbf{G'}(z^{-1})\triangle u(t-1) \tag{31}$$

where terms $\mathbf{y}$, $\mathbf{u}$, $\mathbf{G'}$ and F can be defined in [21]. Equation (31) can be rewritten in this form:

$$\mathbf{y} = \mathbf{G}\mathbf{u} + \mathbf{f} \tag{32}$$

Where $\mathbf{f}$ refers to the last two terms in (31) which only depend on the past. Now, we are able to rewrite (26) as:

$$J = (\mathbf{G}\mathbf{u} + \mathbf{f} - \mathbf{w})^T(\mathbf{G}\mathbf{u} + \mathbf{f} - \mathbf{w}) + \lambda u^T u \tag{33}$$

where $\mathbf{w} = [w(t+d+1), w(t+d+1) \dots w(t+d+N)]^T$

Equation (33) can be written as:

$$J = \frac{1}{2}\mathbf{u^T H u} + \mathbf{b^T u} + f_0 \tag{34}$$

with $\mathbf{H} = \mathbf{2(G^T G} + \lambda\mathbf{I})$, $\mathbf{b^T} = \mathbf{2(f} - \mathbf{w)^T G}$ and $f_0 = (\mathbf{f} - \mathbf{w})^\mathbf{T}(\mathbf{f} - \mathbf{w})$

Therefore, the minimum of *J* can simply be found by making the gradient of *J* equal to zero, which leads to:

$$\mathbf{u} = -\mathbf{H^{-1}b} = (\mathbf{G^T G} + \lambda\mathbf{I})^{-1}\mathbf{G^T}(\mathbf{w} - \mathbf{f}) \tag{35}$$

Since the control signal that is actually sent to the process is the first element of vector $\mathbf{u}$ (receding strategy), it is given by:

$$\triangle u(t) = \mathbf{K}(\mathbf{w} - \mathbf{f}) \tag{36}$$

where $\mathbf{K}$ represents the first element of matrix $(\mathbf{G^T G} + \lambda\mathbf{I})^{-1}\mathbf{G^T}$. Contrary to conventional controllers, predictive ones depend only on future errors and not past ones.

D. Position/torque control strategy for the pneumatic cylinders

The cascade concept for the muscles consists in an outer loop which controls the position and an inner one for the torque. As far as we know, it has been studied in literature in case of the muscles only by [10] and [9]. In our case, we are investigating first the possibility of applying predictive control in such a scheme and the improvement that can be brought by such robust control techniques like GPC and constrained $\mathcal{H}_\infty$. The presented approach is described on Fig. 6. As presented before, the linearized system in case of pressure as an output is an integrator. Therefore, equations of the system can be stated as follows:

$$\begin{aligned} \dot{x} &= (0)x + \begin{pmatrix} 1 & 0 \end{pmatrix}\begin{pmatrix} b \\ v \end{pmatrix} + (1)u \\ \begin{pmatrix} y \\ u \end{pmatrix} &= \begin{pmatrix} -1 \\ 0 \end{pmatrix}x + \begin{pmatrix} 1 & 0 \\ 0 & 0 \end{pmatrix}\begin{pmatrix} b \\ v \end{pmatrix} + \begin{pmatrix} 0 \\ 1 \end{pmatrix}u \\ y &= (1)x + \begin{pmatrix} 0 & 1 \end{pmatrix}\begin{pmatrix} b \\ v \end{pmatrix} + (0)u \end{aligned} \tag{37}$$

where $\omega = (b\ \ v)^T$ and $e = (y\ \ u)^T$ have been defined before. Classical assumptions for solving $\mathcal{H}_\infty$ problem can easily be verified [5]. Using Newton second law yields to the following equation:

$$\tau_m = I_{mov}\ddot{\alpha} + M_{mov}gdcos(\alpha) \tag{38}$$

where α is the rotation angle, I_{mov} represents the inertia of the moving link (in our case it can be the arm with the attached load), d is the distance between the center of rotation and center of mass of moving link, g is the gravity and τ_m the torque generated by the two antagonist muscles. The computed torque [22] consists in the application of the following control signal:

$$\tau_m = I_{mov}v + M_{mov}gdcos(\alpha) \tag{39}$$

where v represents the new control input. Therefore, the obtained linearized system is a double integrator:

$$\ddot{\alpha} = v \tag{40}$$

The GPC controller will be then synthesized based on a double integrator.

For the inner control loop, the objective is to track the reference torque which is set by the outer position controller. In order to set the pressure reference in each muscle, we introduce the pressure average which is defined by:

$$P_m = (P_{m1} + P_{m2})/2 \tag{41}$$

Combining this equation with:

$$\tau_m = F_{m1}(s_1, p_1)s_1(\alpha) - F_{m2}(s_2, p_2)s_2(\alpha) \tag{42}$$

Therefore, using 41, 42 and $s_i = \alpha R$, where R is the radius of the motor between the two muscles. The reference pressure in the second muscle can be calculated by the following relation:

$$P_{2_{ref}} = p_{m_{ref}} - \frac{T_{ref}}{2R\sum_{i=0}^{5} c_i s^i} \tag{43}$$

[5] (A, B_2) controllable and (C_2, A) observable

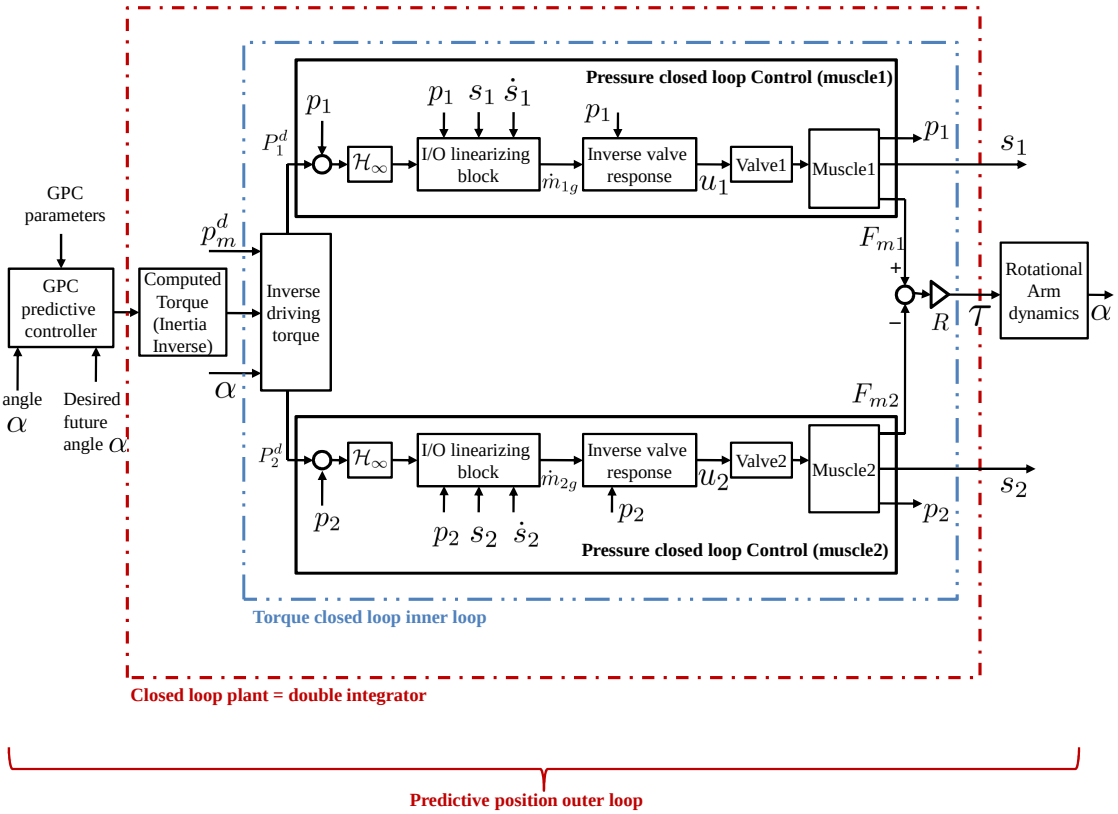

Fig. 6. General block diagram of the cascade Position/torque strategy for the muscles. The inner loop consists in the control of the torque generated by the two muscles. This is done by controlling the pressure in each muscle. An LMI based $\mathcal{H}_\infty$ controller is implemented. The outer loop consists in the computed torque, a position generalized predictive controller is then implemented.

IV. Experimental results

The cascade GPC/$\mathcal{H}_\infty$ is implemented on the PAMs. Nominal tests and robustness are presented respectively.

Some typical tests: On Fig. 7, a test of a square signal with an amplitude of $+/-10^\circ$ and a period of $8s$ is performed. In this test, the arm is not attached yet. The rising time equals $0.113s$ and settling time equals $0.148s$. The overshoot can be accepted because the controller input will never a step of this size in industrial tasks. For the $\mathcal{H}_\infty$ controller, the LMI region for each muscle is a disk centered at $(-100, 0)$ with a radius of 15. The choice of these values is motivated by the fact that big closed pole location values will induce an oscillatory control signal with chattering effect. Small pole values will not insure good tracking results. A tradeoff has to be found. For the synthesis of the position outer controller, the linearized system after computer torque is a double integrator. Therefore, and for a sampling time of $1ms$, polynomials A and B of the CARIMA system introduced in Eq. 25 are given by $A(z^{-1}) = 1-2z^{-1}+z^{-2}$ and $B(z^{-1}) = 5\cdot10^{-7}(1+z^{-1})$. λ is chosen equal to 0.09. The average pressure has been chosen equal to $4bar$. Indeed, there is a relation between the average pressure and the stiffness and consequently, this can have good or bad effects concerning the control performances.

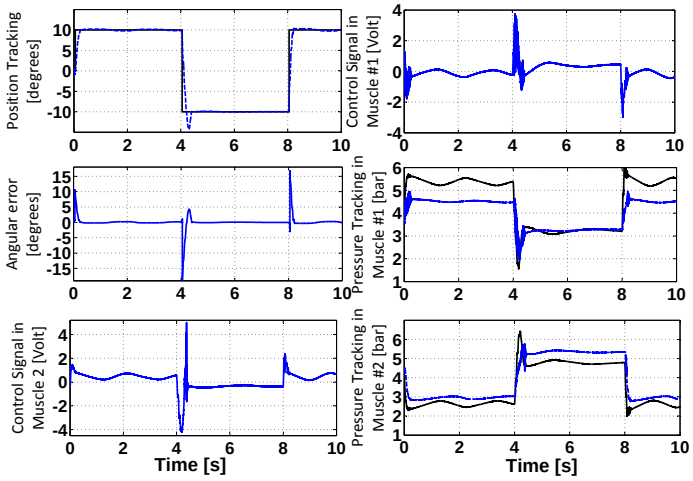

Fig. 7. Pulse response of the muscles in case of a cascade Position/torque control: No load case

In order to evaluate this dependency, two tests with different average pressures and the same control tests are handled. Results are represented in Fig. 8. As related on table I, the

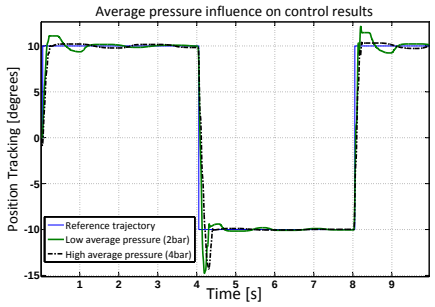

Fig. 8. Studying the effect of the average pressure influence

performances obtained with a high pressure average are better. First, both negative and positive overshoots are reduced in case of $p_m = 4bar$. The same remark can be done for the settling time which is smaller for a high pressure average. The difference is about $0.3s$ which is considerable. These results can be explained by the fact that a high pressure average increases the stiffness of the muscles which can bring an important improvement to the control performances.

However, we are not able to claim that the higher stiffness is

TABLE I
AVERAGE PRESSURE INFLUENCE

	Low average pressure ($p_m = 2bar$)	High average pressure ($p_m = 4bar$)
Rising time (s)	0.075	0.112
Settling time (s)	0.418	0.119
Steady state error (°)	0.04	0.021
Pos. overshoot (%)	10.65	1.9
Neg. overshoot (%)	23.8	21.45

the better the performances are. Indeed some control tests with dynamic reference trajectories have given better results in case of low pressure averages. This can be explained by the fact that in the dynamic case, lower stiffness becomes an advantage for the system in terms of fast reactivity to reference changes. In Fig. 9, a dynamic test with the muscles for a fast sine reference is done. The period equals $T = 2s$ and the amplitude is between $+/-10°$. The maximum error equals $2.24°$ during the switching time and less than $1°$ during the dynamic tracking. On Fig. 10, the arm is attached and a high angle range test is done.. Indeed, one of the drawbacks of muscles is their small contraction capacity which does not exceed 20% of the length. In this $+/-25°$ test, the tracking is insured but the problem for tests with arm is the appearance of vibrations that disturb the performances. Maximum error equals $3.25°$. This elasticity problem of muscles that limits the tracking performances especially for high angle range tests with loads is our big challenge up to now. An asymmetry is observed in the control results, possible explanations can be the friction influence, calibration problems with the valve, gravity effects or a backlash error. These are also some directions that will be investigated in the next months.

Robustness tests: In order to study the robustness of the developed control strategy, the following test is handled. The objective is to study the influence of the time delay for ap-

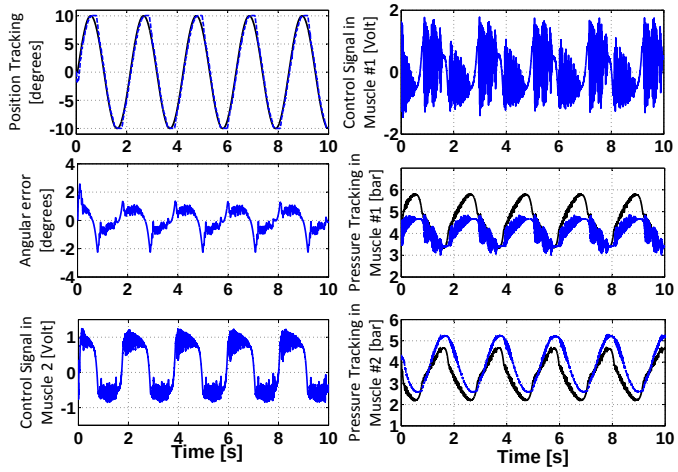

Fig. 9. Sine response of the muscles in case of a cascade Position/torque control

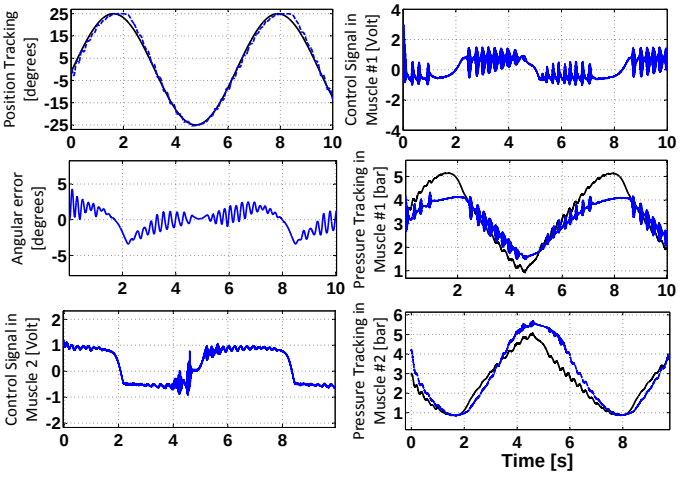

Fig. 10. Dynamic tracking test for the muscles with the attached arm and for high angle ranges $(+/-25°)$

plications where the valves are located far from the actuators. Indeed, one of the advantages of pneumatic actuation is the possible use in explosive environments. This is not true unless the electric auxiliary components - valves and sensors- are mounted far from the actuator. For the test shown in Fig. 11, a $10m$ long flexible tube is added between valve and cylinder. Actually, in parallel robotic applications, the valves will be mounted close to the actuators and this problem of time delay will not be crucial. This explains why time delay has not been included in the model. The objective of this test is just to study the robustness performances of the controller.

Results show effectively a deterioration in performances but stability is maintained and tracking error is always less than $1°$. Another robustness mass variation test is handled. The error signal is represented in figure 12. As a conclusion to this series of tests, following observations comparing to state-of-the-art former results can be made. First, the robust cascade approach

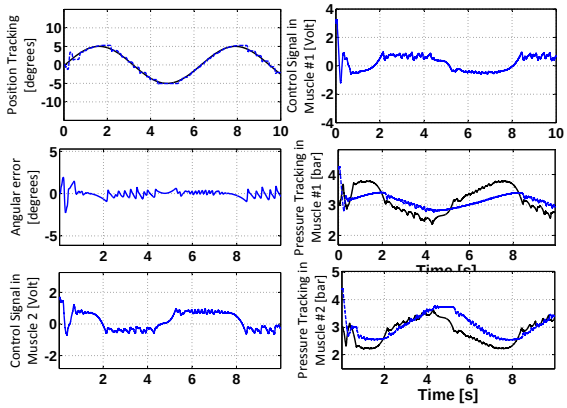

Fig. 11. Robustness position test; valve and pressure sensors have been transferred at $10m$ far from the actuator, vibrations appear but stability is preserved and tracking is still correct with a tracking error less than 1°

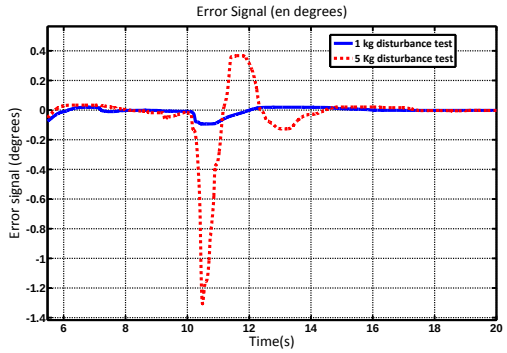

Fig. 12. Robustness mass variation test: a $1kg$ and a $5kg$ loads are added at $t = 10s$.

brings good results in terms of robustness which is a very important requirement in industry. It is possible to track high amplitudes reference signals of $(+/-25^\circ)$ which is substantial regarding to the limited muscle contraction abilities. Finally, another inherent advantage of the proposed approach is that it enables a bigger flexibility in the adjusting of the controller gains as it is possible to act either on the position controller, pressure one and also on the pressure average reference.

V. Conclusion

A robust cascade predictive/$\mathcal{H}_\infty$ control strategy for PAMs is introduced. The goal is to test the muscles for parallel robotics applications. Experimental results have shown good tracking performances and good precision with a static error less of 0.04°. Robustness tests have been also handled and the tracking is still insured when a $10m$ distance exists between valve and actuators. Extended angular displacement tests are experimented for the muscles and give satisfactory results. Future work will concern the elasticity problem which appears for fast tests with $5-10kg$ loads. A possible direction should be a deeper study of the average pressure influence on performances in order to design of optimal average pressure references which insure the best accuracy and robustness performances. Another possibility is to take this elasticity into account explicitly in the model.

Acknowledgment

The authors would like to thank the Fatronik Tecnalia Foundation for its support with the experimental setup.

References

[1] Adept, http://www.adept.com/.
[2] F. Pierrot, C. Baradat, V. Nabat, S. Krut, and M. Gouttefarde. Above 40g acceleration for pick-and-place with a new 2-dof pkm. In *IEEE International Conference on Robotics and Automation, May 12 - 17, Kobe, Japan*, 2009.
[3] M. Van Damme, B. Vanderborght, R. Van Ham, B. Verrelst, F. Daerden, and D. Lefeber. Sliding mode control of a 2-dof planar pneumatic manipulator. *International Applied Mechanics*, 44:1191–1199, 2008.
[4] Xiaocong. Zhu, Guoliang. Tao, Bin. Yao, and Jian Cao. Integrated direct/indirect adaptive robust posture trajectory tracking control of a parallel manipulator driven by pneumatic muscles. *IEEE Transactions of Control Systems Technology*, 17:576–588, 2009.
[5] K. Osuka, Kimura T., and Ono T. H infinity control of a certain nonlinear actuator. In *Proceedings of the 29th Conference on Decision and Control. Honolulu, Hawai*, December 1990.
[6] T. Kimura, S. Hara, and T. Tomisaka. H infinity control with minor feedback for a pneumatic actuator system. In *Proceedings of the 35th Conference on Decision and Control. Kobe, Japan.*, December 1996.
[7] A. Isidori. *Nonlinear Control Systems. Third edition.* Communications and Control Engineering Series. Springer-Verlag, Berlin, 1995.
[8] Michel. Fliess, Jean. Lévine, philippe. Martin, and Pierre. Rouchon. Flatness and defect of non-linear systems: introductory theory and examples. *International Journal of Control*, 61:1327–1361, 1995.
[9] Joachim. Schröder, Kazuhiko. Kawamura, Tilo. Gokel, and Rüdiger. Dillmann. Improved control of a humanoid arm driven by pneumatic actuators. In *International Conference on humanoid Robots*, 2003.
[10] A. Hildebrandt, O. Sawodny, and R. Neumann. Cascaded control concept of a robot with two degrees of freedom driven by four artificial pneumatic muscle actuators. In *American Control Conference. June 8-10, 2005. Portland, OR, USA.*, 2005.
[11] L. Chikh, P. Poignet, F. Pierrot, and C. Baradat. A mixed GPC-$\mathcal{H}_\infty$ robust cascade position-pressure control strategy for electropneumatic cylinders. In *IEEE International Conference on Robotics and Automation. Anchorage, Alaska*, May 3-8, 2010.
[12] Qiang Song and Fang Liu. Improved control of a pneumatic actuator pulsed with pwm. In *Proceedings of the 2nd IEEE/ASME International Conference on Mechatronic and Embedded Systems and Applications*, 2006.
[13] M. Norgaard, P. H. Sorensen, N. K. Poulsen, O. Ravn, and L. K. Hansen. Intelligent predictive control of nonlinear processes using neural networks. In *Intelligent Control, 1996., Proceedings of the 1996 IEEE International Symposium on*, pages 301–306, Dearborn, MI, USA, September 1996.
[14] P. Gahinet, A. Nemirovskii, A.J. Laub, and M. Chilali. The lmi control toolbox. In A. Nemirovskii, editor, *Proc. 33rd IEEE Conference on Decision and Control*, volume 3, pages 2038–2041, 1994.
[15] M. Chilali and P. Gahinet. H-infinity design with pole placement constraints: an lmi approach. *IEEE Transactions on Automatic Control*, 41(3):358–367, March 1996.
[16] G. Duc and S. Font. *Commande Hinf et mu-analyse un outil pour la robustesse*. Hermes, 1999.
[17] K. Zhou and J.C Doyle. *Essentials of Robust Control.* Prentice Hall, 1998.
[18] A. Hildebrandt, O. Sawodny, and R. Neumann. A cascaded tracking control concept for pneumatic muscle actuators. In *European Control Conference 2003 (ECC03), Cambridge UK, (CD-Rom)*, 2003.
[19] M. Belgharbi, S. Sesmat, S. Scavarda, and D. Thomasset. Analytical model of the flow stage of a pneumatic servodistributor for simulation and nonlinear control. In *The Sixth Scandinavian International Conference on Fluid Power. Tampere-Finlande. Pages 847-860.*, 1999.
[20] A.E. Camacho and C. Bordons. *Model Predicitve Control. Second Edition.* Springer, London, 2004.
[21] E.F. Camacho. Constrained generalized predictive control. 38(2):327–332, 1993.
[22] R. J. Schilling. *Fundamentals of robotics, analysis and control*. Prentice Hall, 1990.